Journal of Materials Chemistry A

PAPER

View Article Online
View Journal | View Issue

Cite this: J. Mater. Chem. A, 2018, 6, 5825

Versatile templates from cellulose nanofibrils for photosynthetic microbial biofuel production†

M. Jämsä, ‡[a] S. Kosourov, ‡[a] V. Rissanen, ‡[b] M. Hakalahti,[b] J. Pere,[b] J. A. Ketoja,[b] T. Tammelin *[b] and Y. Allahverdiyeva *[a]

Versatile templates were fabricated using plant-derived nanomaterials, TEMPO-oxidized cellulose nanofibrils (TEMPO CNF) for the efficient and sustainable production of biofuels from cyanobacteria and green algae. We used three different approaches to immobilize the model filamentous cyanobacteria or green algae to the TEMPO CNF matrix. These approaches involved the fabrication of: (A) a pure TEMPO CNF hydrogel; (B) a Ca^{2+}-stabilized TEMPO CNF hydrogel; and (C) a solid TEMPO CNF film, which was crosslinked with polyvinyl alcohol (PVA). The different immobilization approaches resulted in matrices with enhanced water stability performance. In all cases, the photosynthetic activity and H_2 photoproduction capacity of cyanobacteria and algae entrapped in TEMPO CNF were comparable to a conventional alginate-based matrix. Green algae entrapped in Ca^{2+}-stabilized TEMPO CNF hydrogels showed even greater rates of H_2 production than control alginate-entrapped algae under the more challenging submerged cultivation condition. Importantly, cyanobacterial filaments entrapped within dried TEMPO CNF films showed full recovery once rewetted, and they continued efficient H_2 production. The immobilization mechanism was passive entrapment, which was directly evidenced using surface sensitive quartz crystal microbalance with dissipation monitoring (QCM-D). The results obtained demonstrate a high compatibility between CNF and photosynthetic microbes. This opens new possibilities for developing a novel technology platform based on CNF templates with tailored pore-size and controllable surface charges that target sustainable chemical production by oxygenic photosynthetic microorganisms.

Received 21st December 2017
Accepted 12th February 2018

DOI: 10.1039/c7ta11164a

rsc.li/materials-a

Introduction

Cyanobacteria and green algae are widely distributed photosynthetic microorganisms, which are capable of harnessing solar energy and converting it into chemical energy by assimilating atmospheric CO_2. They are considered to be suitable feedstocks for blue biorefineries and attractive biocatalysts for the production of biofuels such as biodiesel, isoprene, alcohols, ethylene and other valuable industrial compounds.[1–3] Theoretical photosynthetic light conversion efficiencies to carbon-based products of approximately 4.6% have been reported,[4] which would satisfy the feasibility of industrial applications. Besides carbon-based biofuels, cyanobacteria and green algae can also produce molecular hydrogen (H_2), which has the highest energy content of reported biofuels and a zero CO_2 release index.[5] These qualities make H_2 an ideal energy carrier for the sustainable bioeconomy of the future. The photosynthetic conversion efficiency to H_2 is much higher than to other carbon-based biofuels. For example, nitrogenase-driven H_2 photoproduction in cyanobacteria has a maximum efficiency of around 6–7%,[6] while direct water biophotolysis in green algae can drive H_2 production with a potential efficiency of 10–12%.[7,8] In reality, however, only a small fraction of these values has been achieved, even in laboratory scale photobioreactors. This is due to various metabolic and production process hurdles, such as the low light utilization efficiency of suspension cultures, sensitivity of photosynthetic organisms to environmental factors, the competition for photosynthetic reductant from wasteful metabolic pathways and the high energy demand of cell cultivation, harvesting and maintenance of photobioreactors.

Thin-layer immobilization is a novel technology recently proposed to ensure uniform light distribution to high-density phototrophic cultures fixed within a controllable volume, and for increasing light-to-product conversion efficiency.[9,10] Besides better light utilization (as compared to suspensions), the entrapment of the dense cultures within the immobilization matrix limits cell division and engages more efficient distribution of photosynthetic reductant to the production of desired end-products, instead of biomass accumulation.

[a]Molecular Plant Biology, Department of Biochemistry, University of Turku, Turku, FI-20014 Finland. E-mail: allahve@utu.fi

[b]VTT Technical Research Centre of Finland Ltd, VTT, PO Box 1000, FIN-02044 Espoo, Finland. E-mail: tekla.tammelin@vtt.fi

† Electronic supplementary information (ESI) available. See DOI: 10.1039/c7ta11164a

‡ These authors contributed equally.

Immobilization also protects the cells from harsh environmental conditions, eases the maintenance of photobioreactors and dramatically prolongs the cultivation period.[11,12] The combination of these factors improves the volumetric and areal productivity of photobioreactors with immobilized photosynthesizing cells. Indeed, Gosse *et al.*[11,13] have recently demonstrated that the entrapment of the phototrophic bacterium, *Rhodopseudomonas palustris* within latex coatings extends the duration of H_2 photoproduction leading to increased H_2-production yields compared to suspension cultures. A similar effect has been demonstrated for H_2-producing green algae[14,15] and heterocystous cyanobacteria[16,17] entrapped within thin Ca^{2+}-alginate hydrogel cubes, beads and films. The improvement of photosynthetic productivity was also confirmed for a few species of cyanobacteria entrapped in the hydrated latex coatings.[18] Although the data are not available, thin-layer immobilization is expected to improve production yields of other bio-based chemicals as well.

Unfortunately, thin-layer immobilization of cyanobacteria and green algae is currently limited to the use of alginate for cellular entrapment. Other materials, such as latex or sol–gel are either toxic to the cells or too expensive for industrial applications. For sustainable production, immobilization matrices are expected to be biodegradable. Although biodegradable, not toxic to the cells and available in industrial quantities, alginates have low mechanical stability and porosity. The low mechanical stability of alginate limits its utilization in long-term applications, especially in media with high contents of phosphates and other chelating agents. Low porosity leads to the accumulation of photosynthetically-evolved O_2 inside the matrix causing photoinhibition and oxidative damage to the entrapped cells, especially under high light conditions.[19] Importantly, the low porosity of alginate also precludes its application as a matrix for the entrapment of designed cyanobacterial or algal cells secreting large molecules (*e.g.* sesquiterpenes).

Cellulose nanofibrils (CNF) offer a range of advantages for the immobilization of cyanobacteria and green algae. CNFs are plant-based building blocks manufactured *via* a so-called top-down approach, which involves disintegration of the plant cell wall structures by chemical/enzymatic and mechanical means.[20] These nanoscaled building blocks are virtually inexhaustible as a source for the construction of renewable, biocompatible and biodegradable materials which are already available in industrial quantities. In this context, the most attractive CNF grade is TEMPO CNF which is produced by TEMPO (2,2,6,6-tetramethylpiperidine-1-oxyl radical)-mediated oxidation of cellulosic fibres.[21] During TEMPO-oxidation, the primary hydroxyl groups of cellulose are selectively converted to anionic sodium C6-carboxylate groups. The release of individual and almost monodispersed nanofibers is achieved with mild mechanical treatment due to electrostatic repulsion. The width of individual fibrils can be as low as 3–5 nm while the length is on the micrometer scale. Due to the small fibril diameter and high aspect ratio, three-dimensional network structures of TEMPO CNF hydrogels are fully transparent, as are the two-dimensional structures of films after the removal of water.[22,23] These qualities allow excellent light penetration. In addition, the nanoscaled fibrillar network brings high porosity coupled with high surface area, enabling the efficient diffusion of vital nutrients and gases, allowing higher cell concentrations in the matrix and offering numerous sites for biomolecules to interact.[24–26] Aforementioned features also improve the mechanical stability of the structures in the presence of water although the CNF based matrices are highly hydrophilic and hygroscopic. Especially when compared to the other biobased materials, CNF gels and films have higher mechanical strength and higher durability in aqueous environments. Several routes to further improve the water stability, CNF gel strength and wet strength of CNF films are available. Gel strength can be improved by *e.g.* gelation with di- or trivalent cations, such as Ca^{2+},[27] whereas TEMPO CNF film wet strength can be enhanced by interfibrillar bridging using *e.g.* polyvinyl alcohol, PVA[28] or by photocrosslinking.[29] Furthermore, tailoring the surface properties and pore size of TEMPO CNF matrices offers controllable cell attachment and facilitated secretion of various chemicals produced by the immobilized cells.

In this work, we investigated several novel approaches to design templates from plant-based TEMPO CNF for the attachment and entrapment of cyanobacterial and green algal cells. Beyond the most essential characteristics which are the photosynthetic activity and the capacity for H_2 production, these biocatalytic templates simultaneously offer a number of vital features such as transparency, flexibility, porosity, and most importantly routes to enhance the water stability. It is important to note that these features are inherently derived from the nanoscaled fibrillar network structure of TEMPO CNF, and that this is in contrast to conventional polymeric biobased materials employed for similar purposes, but for which such a combination has yet to be reported. Our findings reveal the high compatibility of CNF and photosynthetic microbes that were entrapped either in hydrogel layers, or in dry solid films. Water stability of the hydrogels or solid films was improved by ionic crosslinking with Ca^{2+} or by interfibrillar bridging with polyvinyl alcohol. In addition, we provide direct evidence on the mechanisms behind cellular interactions with the CNF matrix and finally suggest a simple strategy, based on electrostatic interactions, to tailor the immobilization mechanism towards even better performance. These findings open new possibilities for developing a novel technology platform with tailored pore-size and controllable surface charge that targets sustainable chemical production by oxygenic photosynthetic microorganisms.

Experimental

Materials

Strains and growth conditions. The Δ*hupL* mutant of filamentous N_2-fixing heterocystous cyanobacterium, *Anabaena* sp. strain PCC 7120 (hereafter, Δ*hupL*) was kindly provided by Prof. H. Sakurai (Waseda University, Japan). The mutant is deficient in the large subunit (accession no. AAC79878.1) of the [Ni–Fe] uptake hydrogenase and, therefore, demonstrates increased hydrogen production yields compared to the wild-type strain.[30] In this study, we always used cells grown under diazotrophic (N_2-fixing) conditions for expression of the nitrogenase enzyme

and following H_2 photoproduction under argon (Ar) atmosphere. The mutant was grown in 1 L Erlenmeyer flasks containing 800 mL Z8x medium,[31] which lacks combined nitrogen. The flasks were placed in a growth chamber at 26 °C and illuminated from two sides with ~60 μmol photons m^{-2} s^{-1} (Photosynthetically Active Radiation, PAR) cool-daylight fluorescent light. The cultures were sparged continuously with sterile air filtered through 0.2 μm pore-size membrane filters (Acro 37 TF, Gelman Sciences, USA). Before immobilization, cyanobacterial filaments were washed once in Z8x medium and pelleted by centrifugation at 3000*g* for 10 min.

The wild-type green alga, *Chlamydomonas reinhardtii* (hereafter, *C. reinhardtii*) strain CC-124 (mt−, nit−) was obtained from the Chlamydomonas Resource Center at the University of Minnesota, USA. The alga was grown under the same conditions as the Δ*hupL* mutant, but on the standard Tris-Acetate-Phosphate (TAP) medium.[32] Prior to immobilization, *C. reinhardtii* cells were sulfur-depleted to initiate H_2 photoproduction.[33] For this, algal cultures were grown to the late logarithmic phase (~25 μg total Chl per mL), harvested by centrifugation at 3000*g* for 3 min, washed once in TAP-minus-sulfur-minus-phosphorus (TAP-S-P) medium to remove sulfates and phosphates, and pelleted by centrifugation prior to entrapment in TEMPO CNF and alginate hydrogels. Since green algal hydrogel layers were submerged into the medium, exclusion of phosphates from the medium helps to prevent dissolution of the Ca^{2+}-stabilized hydrogel matrices.

TEMPO-oxidized cellulose nanofibrils (TEMPO CNF). Never-dried bleached softwood pulp (spruce/pine mix) obtained from a Finnish pulp mill was used as a raw material for the production of cellulose nanofibrils. TEMPO-mediated oxidation of the pulp fibers was carried out by alkaline oxidation with hypochlorite catalysed by TEMPO, according to the procedure described by Saito *et al.*[21] The anionic charge of the oxidated pulp was 1.28–1.41 mmol g^{-1}, as determined with a standard conductometric titration method (SCAN 65:02). After the TEMPO-oxidation the pulp was washed and fibrillated into CNF (hereby called TEMPO CNF) in a microfluidizer (Microfluidics Int., USA) equipped with two Z-type chambers with respective diameters of 400 and 100 μm. The fibrillation was done in two passes at 1850 bar operating pressure, and the final consistency of the TEMPO CNF was *ca.* 1 wt%. The appearance of TEMPO CNF is a viscous and transparent hydrogel (light transmittance of 74.3% at 800 nm by UV-Vis spectroscopy).[23] The carbohydrate composition of TEMPO CNF is 64.0% glucose, 6.2% xylose and 2.1% mannose.[34] Fig. 1 shows the transparent and flexible appearance, topography and morphology of self-standing TEMPO CNF film, in comparison with Ca^{2+}-alginate film, which was used as a reference material.

Polymers. Sterile 4 wt% alginate solution used as a reference matrix was prepared by mixing Na-alginate salt from brown algae (#71238, Sigma-Aldrich) in Milli-Q water and by autoclaving the mix at 121 °C for 10 min. Polyvinyl alcohol (Mowiol 56-98, Mw 195 000 g mol^{-1}, DP 4300) used as a CNF film wet strength additive was purchased from Sigma-Aldrich and dissolved to a 5 wt% solution in Milli-Q water at 95 °C. Branched polyethylene imine (M_w 70 000 g mol^{-1}, 30 wt% aqueous solution) used as anchoring polymer for CNF thin films was purchased from Polysciences and used as received.

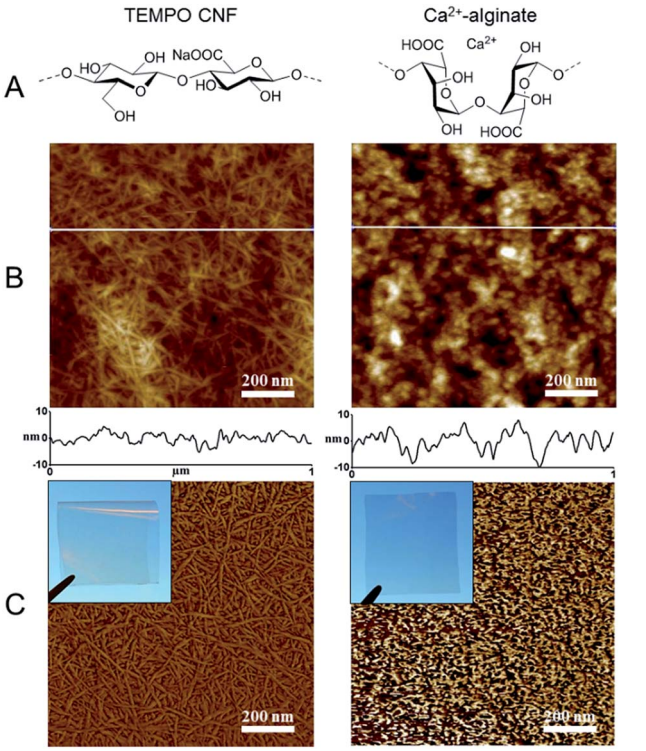

Fig. 1 Chemical composition and morphology of the matrices. (A) Chemical structure of TEMPO CNF (left) and Ca^{2+} alginate (right). (B) 1 μm × 1 μm AFM topography images with the height profile scans (white line) of solid TEMPO CNF film (left) and Ca^{2+}-alginate film (right) with (C) corresponding AFM phase contrast images. Visual appearance of the films is shown in the inset photographs.

Other chemicals and materials. All chemicals were of analytic grade and used as received. 2,2,6,6-Tetramethylpiperidin-1-oxyl (TEMPO), sodium bromide (solid) and 10% sodium hypochlorite (aqueous) were purchased from Sigma-Aldrich. 0.1 M sodium hydroxide solution was obtained from Fluka Analytical. $CaCl_2$ (99%, #C7902) was purchased from Sigma-Aldrich. Ultrapure water (18.2 MΩ cm) was prepared with a Milli-Q purification unit (QPAK® 1, Millipore). Whatman® cellulose blotting paper (3MM Chr, #3030-931, Sigma-Aldrich) was used as a support. For submerged cultivation of Ca^{2+}-hydrogels, instead of blotting paper, a plastic 120 μm-thick insect screen support was applied. Melamine foam sponge was cut into 3 × 1 × 1 cm pieces and boiled in Milli-Q water for 1 h before use. QCM-D experiments were performed on AT-cut quartz crystal sensors with gold electrodes purchased from Q-sense AB (Gothenburg, Sweden), with a fundamental resonance frequency of 5 MHz and a sensitivity constant of 0.177 mg m^{-2} Hz^{-1} as reported by the supplier.

Methods

Immobilization procedures

Approach A: TEMPO CNF hydrogel layers. The cyanobacterial filaments were entrapped within thin hydrogel layers, which

were formed on top of the blotting paper support. The Δ*hupL* pellets were mixed in 1 : 1 wet-mass ratio with different hydrogels: (i) 1 wt% TEMPO CNF; (ii) 1 wt% TEMPO CNF and 0.1 wt% polyvinyl alcohol (PVA); and (iii) 4 wt% alginate as a control. In the second formulation, PVA, which was used as a crosslinker in following studies, was added to investigate its biocompatibility with the cyanobacteria. The hydrogel layers were formed by drawing down the formulations with a stainless steel rod over the blotting paper to produce uniform layers (Fig. 2A). Finally, the layers were cut into 3 × 1 cm strips and placed on top of 3 × 1 × 1 cm melamine foam sponges that supply water to the strips. The sponges with strips were placed inside 33 mL gas-tight vials filled with 5 mL Z8x medium. The strips were incubated at 26 °C under Ar atmosphere containing 6% CO_2 and light intensity of 140 μmol photons m^{-2} s^{-1} PAR. It is important to note that all previous studies on thin-layer immobilization of cyanobacteria and green algae were performed with Ca^{2+}-alginate hydrogel films. For the sake of comparison, we therefore applied Ca^{2+} to alginate polymers in all immobilization approaches mentioned here and below.

Approach B: TEMPO CNF hydrogel layers crosslinked with Ca^{2+}. Algal Ca^{2+}-stabilized TEMPO CNF hydrogel layers were produced on top of the template consisting of a white-polymer insect screen placed over the sticky side of a Scotch-type tape (Fig. 2B) as described before.[14] The insect screen was embedded in the hydrogel layers for improving their mechanical stability. Sulfur-depleted *C. reinhardtii* pellets were mixed in 1 : 1 wet-mass ratio with (i) 0.5 wt% TEMPO CNF, (ii) 0.5 wt% TEMPO CNF + 0.05 wt% PVA and (iii) 4 wt% Ca^{2+}-alginate as a control. The algal hydrogel layers were formed as described in the approach A. In contrast to the approach A, both TEMPO CNF and alginate hydrogel matrices were stabilized by spraying the surface with 50 mM $CaCl_2$ solution. The Ca^{2+}-stabilized hydrogel layers were washed in Milli-Q water, cut into 6 × 1 cm strips and submerged into 10 mL TAP-S-P medium in 75 mL gas-tight vials. In the beginning of each experiment, the gas phase in the

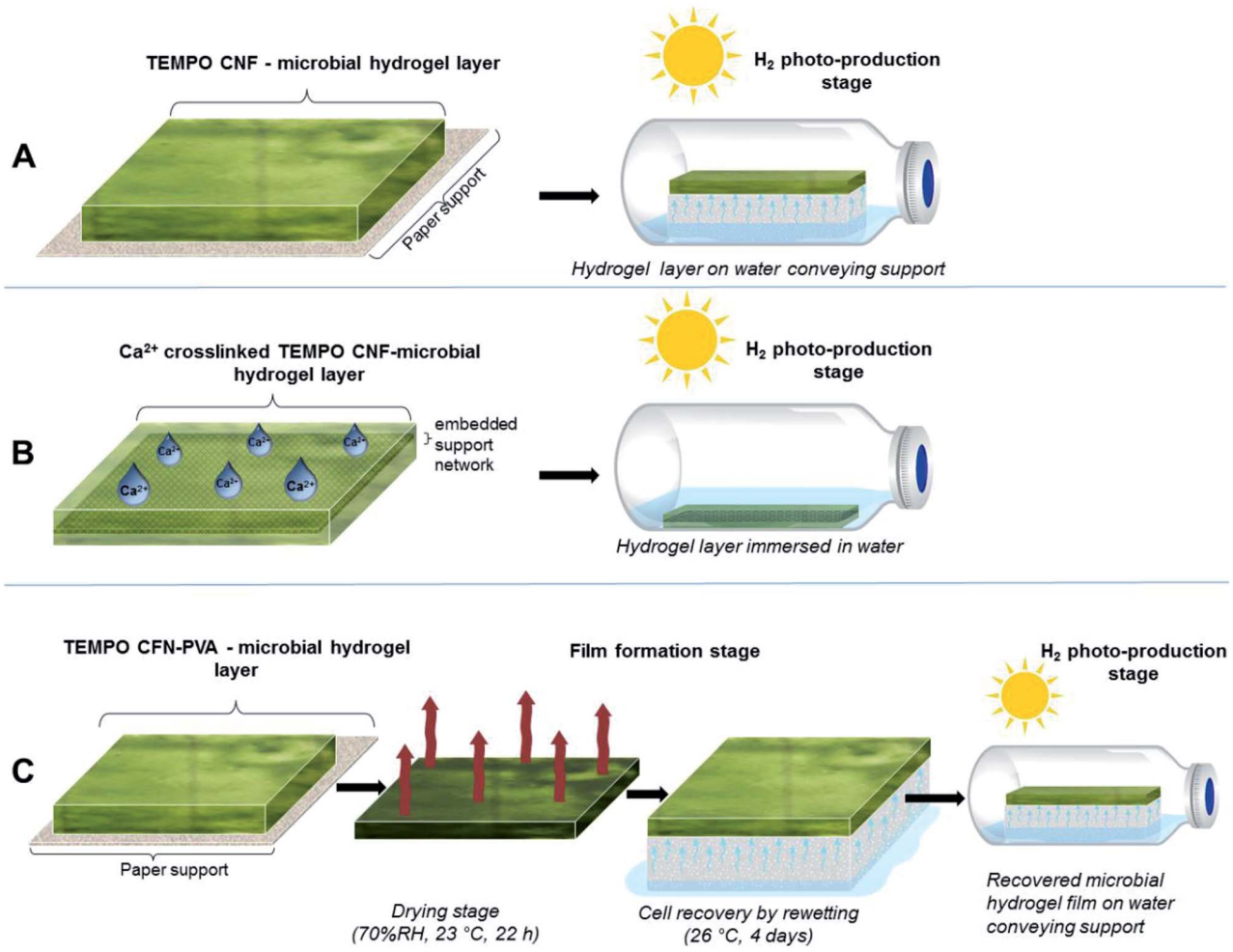

Fig. 2 Schematic representation of immobilization approaches for H_2 photoproduction. (A) TEMPO CNF-microbial hydrogel layers with entrapped cyanobacteria applied on top of the paper support and placed in the gas-tight vials above the medium on top of water conveying sponge that provides water to the cells *via* capillary actions. (B) Ca^{2+}-stabilized TEMPO CNF hydrogel layers with entrapped algae with embedded support network submerged into the cultivation medium. (C) PVA containing TEMPO CNF hydrogel layers with entrapped cyanobacteria applied on paper support with the drying and recovery steps. During the drying step, the solid film is formed, and PVA forms interfibrillar bridges with TEMPO CNF that enhance the film wet strength. Photoproduction set up is similar to the approach A.

vials was replaced to pure Ar. The vials were incubated at 26 °C under fluorescence light of 50 μmol photons m^{-2} s^{-1} PAR.

Approach C: dry PVA-crosslinked TEMPO CNF films with immobilised cyanobacteria and recovery by re-wetting. The Δ*hupL* PVA-crosslinked TEMPO CNF films were formed by drying the hydrogel layers (prepared as described in the approach A) on the top of the paper support for 22 h in complete darkness at 23 °C and 70% relative humidity (Fig. 2C). The hydrogel formulations consist of cell wet biomass mixed in either 1 : 1 or 1 : 2 mass ratio with 0.5 wt% TEMPO CNF supplemented with 0.05 wt% PVA. The Ca^{2+}-stabilized alginate hydrogel films (made of 4 wt% alginate solution without PVA) were served as a positive control, while the matrix-free cell biomass placed on top of the paper support was used as a negative control.

The Δ*hupL* cells in dried films were recovered by placing the film on top of the melamine foam sponge, which supplied Z8x medium to the entrapped cells. The recovery was done in closed Petri dishes at 26 °C under air atmosphere supplemented with 0.5% CO_2. During the 4 days recovery, strips were illuminated with 6 μmol photons m^{-2} s^{-1} PAR. After the recovery stage, the film-coated paper was cut into 3 × 1 cm strips and strips were transferred into the 33 mL gas-tight vials containing 5 mL Z8x medium. To initiate efficient H_2 photoproduction by the Δ*hupL* cells, the headspace of the vials was replaced to Ar and supplemented with 6% CO_2. The PVA-crosslinked TEMPO CNF and Ca^{2+}-alginate films were top-illuminated with 140 μmol photons m^{-2} s^{-1} PAR.

Photosynthetic activity monitoring. The photosynthetic activity of the immobilized cells was monitored with PAM-2000 (Walz, Germany). Cells were dark adapted for 3 min before the activity measurements. Red actinic light (655 nm) of 84 μmol m^{-2} s^{-1} was applied for 210 s and saturating white light pulses (0.8 s) of 2000 μmol m^{-2} s^{-1} PAR were fired every 20 s to determine F'_m, the maximum fluorescence under actinic light. The effective yield of Photosystem II (YII) were calculated as $(F'_m - F_s)/F'_m$, where F_s is steady-state fluorescence under actinic light.

Determination of H_2 and O_2 contents. The H_2 and O_2 concentrations in the headspace of the vials were monitored using Clarus 500 gas chromatograph (PerkinElmer, Inc.) equipped with a thermal conductivity detector and a molecular sieve 5 A column (60/80 mesh). 150 μL samples were taken with a gas-tight 250 μL gas chromatography syringe (Hamilton, USA) equipped with a sample lock.

Detection of TEMPO CNF and cyanobacteria interactions by QCM-D. Attachment of cyanobacteria to the surface of TEMPO CNF thin films was investigated with Quartz Crystal Microbalance with Dissipation Monitoring (QCM-D) using the Q-Sense E4 instrument equipped with an Open Module 401 (Q-Sense AB, Gothenburg, Sweden), which allows direct application of desired sample solutions onto the sensor surface. The QCM-D instrument allows *in situ* detection of mass changes between solid–liquid or solid–gas interfaces. A detailed interpretation of QCM-D measurement data can be found elsewhere,[35,36] and is briefly described in ESI.†

The preparation of supported TEMPO CNF thin films with a typical thickness of circa. 10 nm [34] on QCM-D sensors was performed according to the procedure described by Eronen *et al.*[37] with slight modifications as described by Hakalahti *et al.*[34] and is described in ESI.†

Cationization of TEMPO CNF films was carried out by drop casting 200 μL of 1 mg mL^{-1} PEI solution in Milli-Q water onto the surfaces for 30 min, followed by rinsing with Milli-Q water and drying with N_2 gas.

Prior to the cyanobacteria attachment experiments the TEMPO CNF surfaces (anionic TEMPO CNF and cationized TEMPO CNF) were stabilized by immersing in Z8x medium for 16 hours. The surfaces were then quickly dried with N_2 gas and inserted into the QCM-D Open Module (QOM 401) cell. Schematics for different cyanobacteria attachment protocols involving anionic TEMPO CNF surface and cationized TEMPO CNF surface are presented in Fig. 3. First, 250 μL of Z8x medium was pipetted directly onto the surface and Δ*f* and Δ*D* values were monitored until a stable baseline was achieved. Stable baselines were attained within 1 hour. After stabilization, the medium was changed to 250 μL *Anabaena* Δ*hupL* suspension ($OD_{720} \approx 0.1$, corresponding to dry weight percent of 0.05 wt%) in Z8x medium, and again Δ*f* and Δ*D* values were monitored for 2 h. Finally, the surfaces were rinsed with Z8x medium by sequential removal and addition of 250 μL of the medium until no changes in frequency and dissipation values were observed. After the measurements, the crystals were dried with N_2 gas and stored in desiccator in darkness.

The estimation of final areal mass of the attached Δ*hupL* filaments on TEMPO CNF surface was determined as described by Peresin *et al.*[38] with some modifications, by following the difference in frequency response of the sensor. The measurement was carried out with the QCM-D Flow Module (QFM 401) in air at 23 °C, and is described further in ESI.†

Complementary analytical methods. Optical microscopy imaging of TEMPO CNF thin films with attached cyanobacteria was performed using a Nikon eclipse Ci-L microscope with a Nikon DS-Fi2 digital camera (Nikon, Melville, NY, USA).

Scanning electron microscopy (SEM) imaging of TEMPO CNF-PVA and Ca^{2+}-alginate films (Approach C) was performed with Zeiss Merlin FE-SEM (Carl Zeiss AG, Oberkochen,

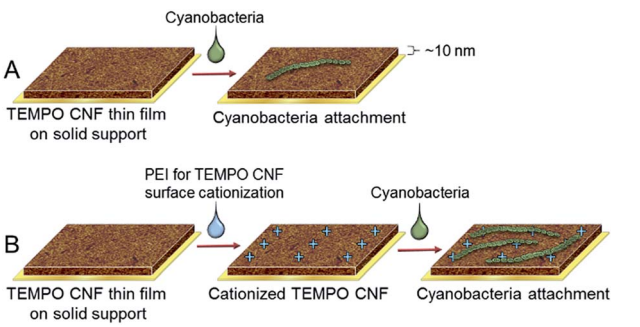

Fig. 3 Scheme of the QCM-D experiments to investigate the immobilization mechanisms of cyanobacteria filaments on TEMPO CNF surface. (A) Filament attachment on anionic TEMPO CNF and (B) filament attachment on cationized TEMPO CNF. Cationization was carried out by drop casting cationic PEI on TEMPO CNF prior introducing the cyanobacteria filaments.

Germany), with 2 keV accelerating voltage. The samples were coated with platinum with a sputter-coater (20 mA for 30 seconds) to improve the conductivity of the samples and thus the quality of the SEM images.

Atomic force microscopy (AFM) imaging of the CNF surfaces was performed with ANASYS AFM+® (ANASYS Instruments Inc., Santa Barbara, CA USA). The images were taken in tapping mode in air using aluminium coated n-type silicon cantilevers (HQ:NSC15/Al BS, Micromasch, Tallinn, Estonia) with typical probe radius of 8 nm, force constant of 40 N m^{-1} and nominal resonance frequencies between 265 and 410 kHz. The images were not processed in any way.

For Chl *a* determination in cyanobacteria, the strips were incubated in 90% aqueous methanol at 65 °C for 30 min. The Chl *a* content in methanol extracts was determined spectrophotometrically using extinction coefficient given by Lichtenthaler.[39] The total Chl (*a* + *b*) in green algal samples was determined in 95% ethanol extracts as described before.[19]

Results and discussion

We used three different approaches for the immobilization of the filamentous cyanobacterium, Δ*hupL* and the green alga, *C. reinhardtii* within thin TEMPO CNF matrix layers (see Fig. 2 and methods for more details). In the first approach, Δ*hupL* was entrapped within TEMPO CNF hydrogel layers. For improving H_2 photoproduction yields of N_2-fixing filaments, the hydrogels with entrapped Δ*hupL* were placed in gas-tight vials and the head-space was changed to Ar + 6% CO_2.[16] In the second approach, green algal cells were entrapped within TEMPO CNF hydrogel layers, which were additionally crosslinked with Ca^{2+} following the protocol developed for sulfur-deprived *C. reinhardtii* cultures.[14] Here, sulfur-deprivation was applied for initiation of H_2 production activity in algal cells.[33] These two approaches allowed for evaluation of the biocompatibility and suitability of TEMPO-oxidized CNF matrices for the immobilization of cyanobacteria and green algae. The third approach was applied for improving the mechanical stability of the TEMPO CNF matrices. PVA-crosslinked TEMPO CNF films with entrapped Δ*hupL* filaments were formed, dried and checked for H_2 photoproduction activity, following a 4 d re-wetting period. The third approach was also applied to *C. reinhardtii* without success and, therefore, is not described in this paper.

Approach A: TEMPO CNF hydrogels demonstrate cyanobacterial biocompatibility similar to alginate

In order to evaluate biocompatibility of TEMPO CNF for the immobilization of cyanobacteria, Δ*hupL* filaments were entrapped within thin TEMPO CNF and TEMPO CNF-PVA hydrogel layers (Fig. 2A). Photosynthetic and H_2 photoproduction activities were compared to the filaments entrapped in alginate hydrogels. The Ca^{2+}-alginate polymer is known as a suitable, but not very mechanically stable carrier for thin-layer entrapments of H_2-producing cyanobacteria[16] and green algae.[14] In addition, the hydrogel layers with entrapped filaments were compared with the matrix-free cells applied directly on the top of the paper support.

As shown in Fig. 4A, CNF hydrogels with entrapped Δ*hupL* filaments yielded similar amounts of H_2 as the alginate-entrapped and the matrix-free filaments exposed to the same conditions. The maximum specific rates were slightly higher in TEMPO CNF and TEMPO CNF-PVA hydrogels as compared to alginate or matrix-free samples, being 18.0 ± 0.7, 18.3 ± 0.9, 13.7 ± 1.3, 13.0 ± 0.3 μmol H_2 (mg Chl h)$^{-1}$, respectively. The difference between samples was statistically significant ($P < 0.05$). In addition, all the samples showed similar effective Photosystem II yield and net O_2 evolution (Fig. S1†). These data indicate the biocompatibility of TEMPO CNF and TEMPO CNF-PVA matrices for the immobilization of cyanobacteria. Indeed,

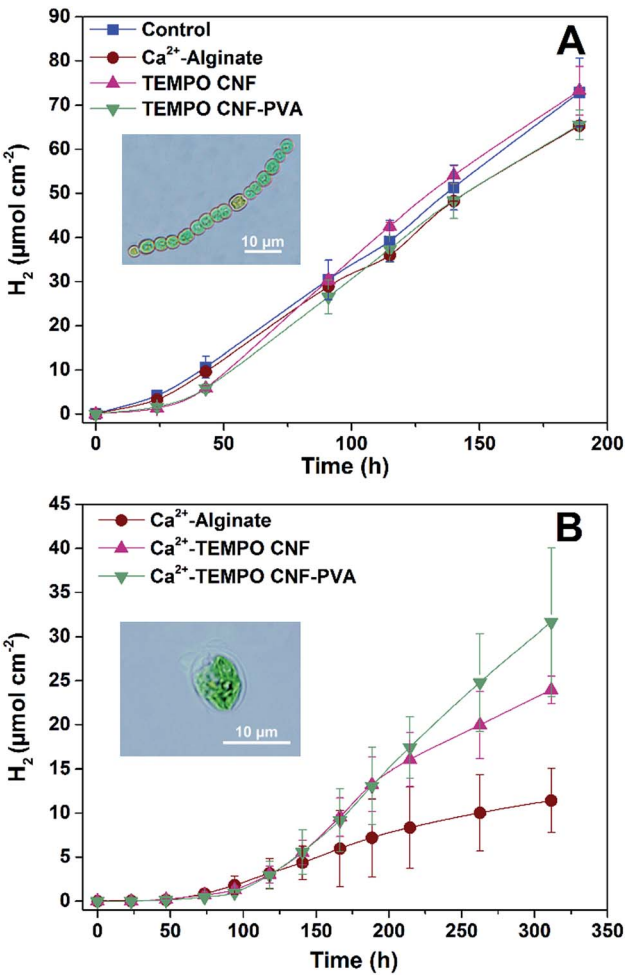

Fig. 4 H_2 production yields by filamentous cyanobacteria and green alga entrapped in hydrogel layers using approach A and B, respectively. (A) Cyanobacterial filaments entrapped in different hydrogel layers: control – matrix-free cyanobacterial filaments; Ca^{2+}-alginate – cyanobacterial filaments entrapped 4 wt% alginate hydrogel stabilized with 50 mM $CaCl_2$; TEMPO CNF – 1 wt% TEMPO CNF; TEMPO CNF-PVA – TEMPO CNF with 0.1 wt% PVA. (B) Algal cells entrapped in different hydrogel layers: alginate – 4 wt% alginate; Ca^{2+}-TEMPO CNF – 0.5 wt% TEMPO CNF; Ca^{2+}-TEMPO CNF-PVA – 0.5 wt% TEMPO CNF with 0.05 wt% PVA. Cells and matrix formulas were mixed in 1 : 1 wet-mass ratio. Each experimental point represents three replicates, and the error bars are standard deviation.

the activity of CNF immobilized cells was slightly increased compared to alginate-entrapped and matrix-free cells.

Approach B: algal Ca^{2+}-crosslinked TEMPO CNF hydrogel layers yield more H_2 than alginate-entrapped algae

Similar to alginate, TEMPO CNF hydrogels can be stabilized by di- or trivalent metal ions such as Ca^{2+}, Ba^{2+}, Al^{3+} and Fe^{3+}. The cations draw adjacent fibrils together, which prevents water molecules from solvating their surface, increasing their mechanical stability in water.[27] Hence, in order to create hydrogel layers with increased performance in a submerged state, the layers with entrapped *C. reinhardtii* cells were stabilized by Ca^{2+} and placed in sulfate/phosphate-free medium in the vials under an Ar atmosphere. Here, algae entrapped in CNF hydrogels yielded more H_2 than the cells entrapped in alginate (Fig. 4B), but all samples showed similar effective Photosystem II yield in the beginning and at the end of the experiment (Fig. S2†). The effect was most likely due to the different structures of the materials in the nanoscale (Fig. 1). The TEMPO CNF hydrogel is formed by a highly porous fibrillar network,[26] whereas alginate hydrogels possess a more granular structure. This suggests lower porosity for alginate, which may restrict H_2 photoproduction by limiting diffusion of H_2 from the alginate layers. In contrast to nitrogenase-dependent irreversible H_2 evolution in heterocystous cyanobacteria, the [FeFe]-hydrogenase enzyme in green algae catalyses a reversible reaction of H_2 production. Therefore, we hypothesise that accumulation of H_2 inside the alginate matrix would increase the back reaction (H_2 uptake) in algal cells. This is in line with studies showing that the H_2 photoproduction yield in *C. reinhardtii* declines with increased H_2 partial pressure.[40,41]

Approach C: solid cyanobacterial TEMPO CNF films recover biocatalytic activity after drying

To further increase the mechanical stability and wet strength of the hydrogel films, the cyanobacterial TEMPO CNF-PVA hydrogels were exposed to a drying process for 22 h at 23 °C and 70% relative humidity. Drought stress is known to reduce cyanobacterial cell fitness and strongly decrease photosynthetic activity.[42] For evaluating the possible inhibition/recovery of photosynthetic apparatus throughout the film formation process, we monitored the effective Photosystem II yield of the entrapped Δ*hupL* filaments. As expected, photosynthetic activity dramatically declined upon drying in all studied films (Fig. 5A). However, the re-wetting phase (Fig. 5B) allowed a gradual recovery of photosynthetic activity. On the third and fourth days of re-wetting, cyanobacteria entrapped in thin films demonstrated a similar photosynthetic activity as observed initially. As opposed to the entrapped cyanobacteria, the matrix-free control filaments could only partially recover to about 60% of the initial effective Photosystem II yield (Fig. 5B) and 55% of the initial Chl *a* level (Table S1†).

The better recovery in TEMPO CNF films may be explained by the hygroscopic structure of the material. Due to the inherent hygroscopic properties of the nanoscaled fibrillar network matrix, TEMPO CNF films still contain structural water as multilayers and clusters at 70% RH,[34] and this moisture protects cyanobacterial filaments during drying.

After the full four-day recovery period, Δ*hupL* solid films were subjected to conditions favourable to H_2 photoproduction (Ar + 6% CO_2). As shown in Fig. 5C, the Δ*hupL* filaments entrapped within 4 wt% alginate films yielded the highest H_2 amount by the end of the ~9 d (211 h) experiment. Among CNF formulations, the films with higher matrix to biomass ratio showed better H_2 production yields, most likely due to a better cell recovery (Table S1†).

Importantly, during the recovery stage, the kinetics and amplitude of the inhibition and recovery processes were similar in TEMPO CNF-PVA and alginate films, suggesting applicability of these solid films as a novel technology platform.

Revealing the interactions between cyanobacteria and TEMPO CNF using QCM-D

Immobilization mechanisms and the interactions between TEMPO CNF and cyanobacteria were revealed using quartz crystal microbalance with dissipation monitoring (QCM-D). QCM-D measurements provide quantitative information on phenomena taking place at solid–liquid and solid–air interfaces, enabling the determination whether the cyanobacterial filaments are attached to the TEMPO CNF fibrils, or merely passively entrapped in the matrix.

Here we investigated the interactions of Δ*hupL* filaments to TEMPO CNF using a specifically developed Open Module QCM-D measurement cell. With this set up, the filament-containing liquid sample is directly pipetted on the fibril covered sensor surface and, thus, sensitive biomolecules with large size distribution can be introduced without *e.g.* pumping through the thin tubing. Fig. 6A shows the changes in frequency (Δf) and dissipation (ΔD), which occurred due to changes in mass and viscoelastic properties monitored at solid–liquid interface of the TEMPO CNF ultra thin film. First, the TEMPO CNF surface was stabilized in the growth medium (Fig. 6A, buffer stabilization step) for 1 h in order to attain a more or less stable baseline. This step was followed by the introduction of the cyanobacterial suspension. Sharp changes in both Δf and ΔD signals were observed, due to the mechanical stress caused by the change of liquid, which was directly pipetted onto the QCM-D sensor surface. Attachment of cyanobacteria on the TEMPO CNF surface was monitored for 2 h and the system was then rinsed again with pure buffer medium in order to remove unattached filaments. The minor negative change in frequency of −5.8 Hz indicates that cyanobacteria filaments do not spontaneously attach to TEMPO CNF surface.

To further investigate the interactions between TEMPO CNF and cyanobacteria, mass changes were assessed at the solid–air interface under dry conditions (Fig. 6B). Here, the change in frequency was monitored before and after the cyanobacteria attachment step, after buffer rinsing. At the solid–air interface the frequency change (Δf) was −32 Hz, corresponding to an increase in areal mass (Δm) of 560 ng cm^{-2} according to the Sauerbrey equation (eqn (1) in ESI†). The results indicate that minor filament attachment occurs when the filaments are

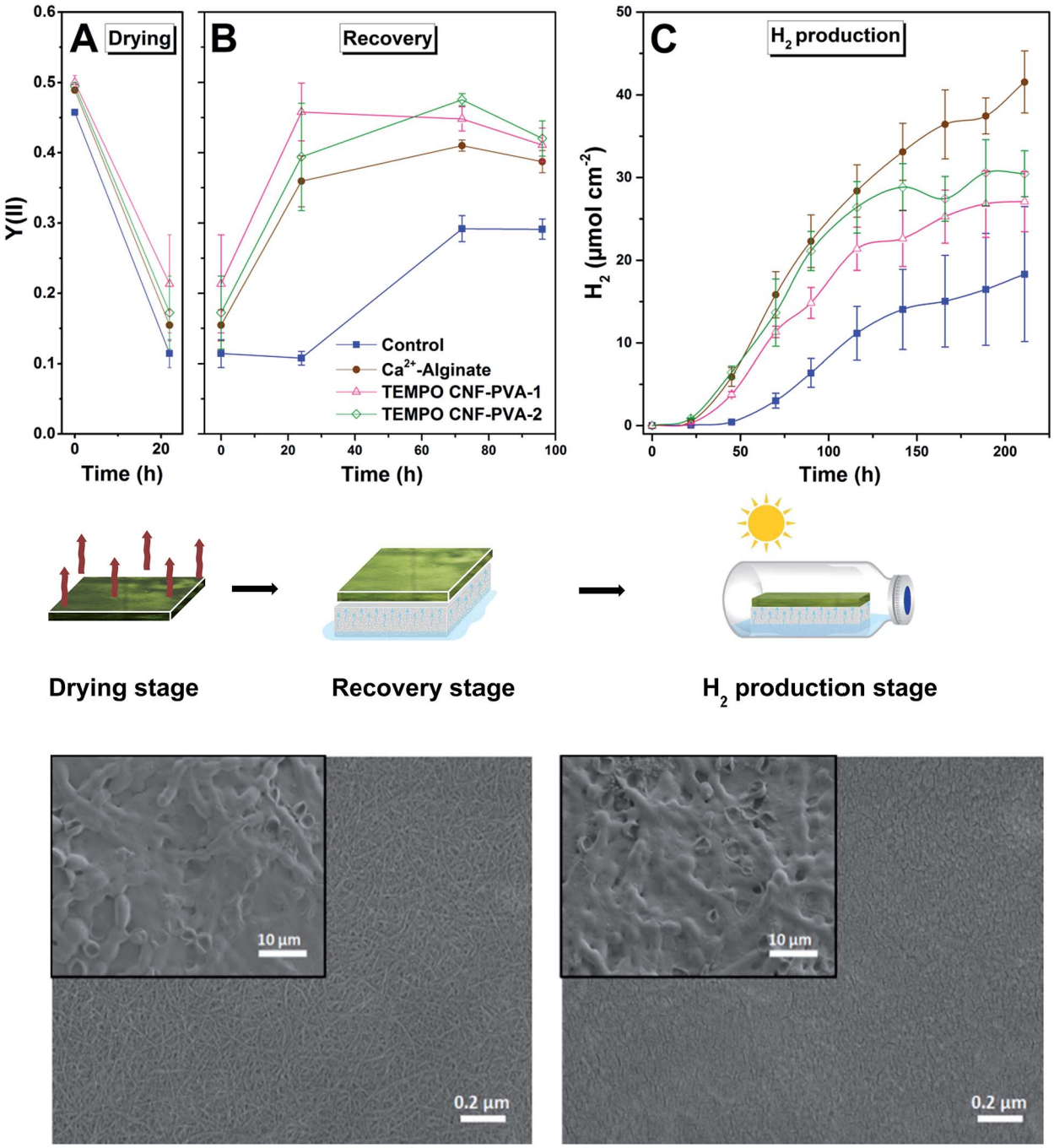

Fig. 5 Entrapment of cyanobacterial cells in solid PVA-crosslinked TEMPO CNF films using the approach C. The photosynthetic activity Y(II) of the cyanobacterial cells entrapped in TEMPO CNF-PVA hydrogels during the drying (A) and recovery (B) stage of film formation experiment. Hydrogen yields (C) from the following anaerobic hydrogen production stage. Control – matrix-free cyanobacterial filaments; Ca^{2+}-Alginate – cyanobacterial filaments entrapped in 4 wt% alginate hydrogel with matrix–cell wet mass ratio of 1 : 1 stabilized with 50 mM $CaCl_2$; TEMPO CNF-PVA-1 – 0.5 wt% TEMPO CNF with 0.05 wt% PVA with matrix–cell wet mass ratio of 1 : 1; TEMPO CNF-PVA-2 – 0.5 wt% TEMPO CNF with 0.05 wt% PVA with matrix–cell wet mass ratio of 2 : 1. SEM images with different magnifications show the appearance of solid films of PVA crosslinked TEMPO CNF (left) and Ca^{2+}-crosslinked alginate (right) with entrapped cyanobacteria.

forced to approach at close proximity to TEMPO fibrils, due to removal of the buffer. Strong and spontaneous attachment is prevented by the overall anionic surface charges of TEMPO CNF and the Δ*hupL* filaments at neutral pH.[43,44]

As shown in Fig. 4 and 5, highly anionic TEMPO CNF provides a good immobilization matrix for cyanobacteria and green algae with good H_2 production yields, although the immobilization mechanism in this case appears to be a passive entrapment. However, the direct attachment of cells to the surface of the solid matrix support creates a natural and less-invasive route to whole-cell immobilization,[45] which mimics the natural biofilm formation process.[46,47] Due to the direct

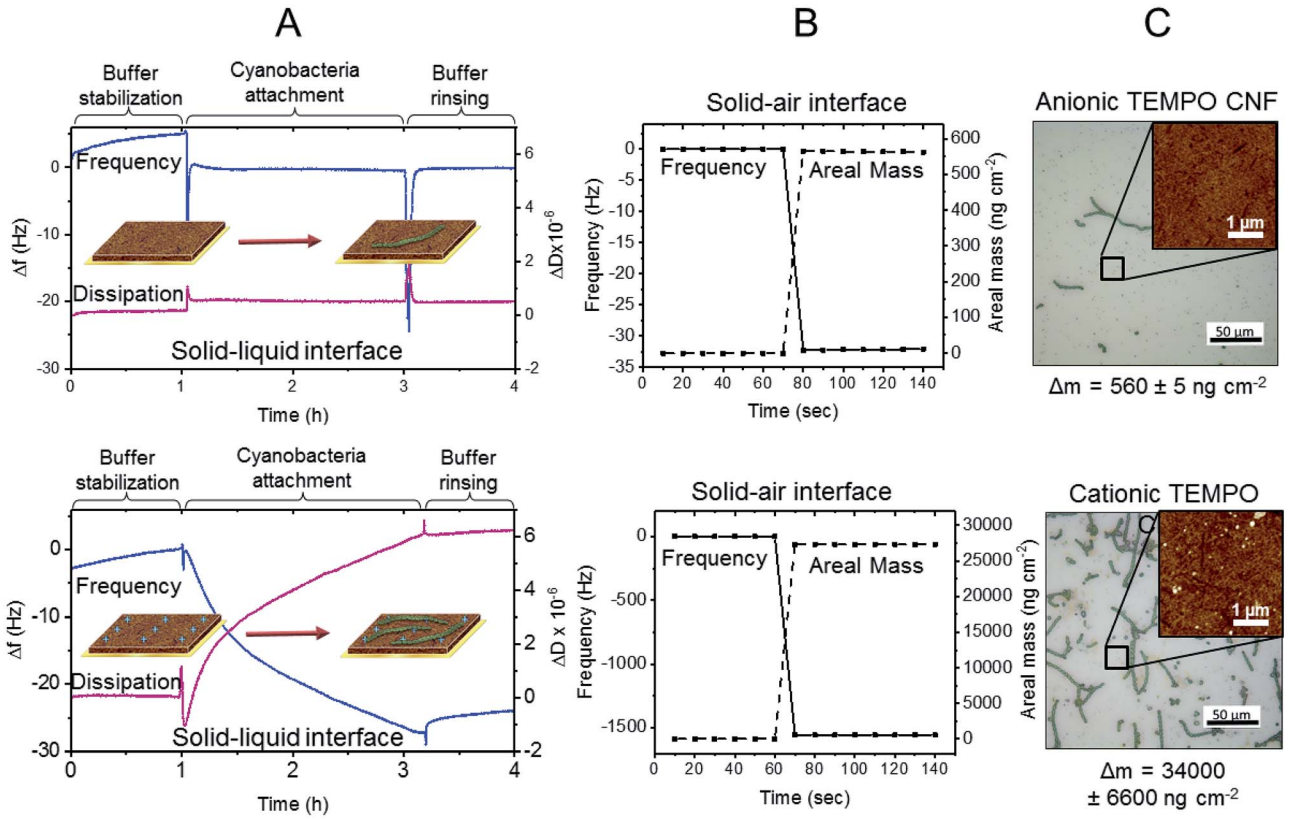

Fig. 6 Interactions between cyanobacteria and TEMPO CNF. (A) Change in frequency and dissipation monitored at solid–liquid interface during cyanobacteria attachment on anionic TEMPO CNF (top) and on cationized TEMPO CNF (bottom) as a function of time measured by QCM-D (f_0 = 5 MHz, n = 7, f_7 = 35 MHz). (B) Change in frequency and areal mass calculated by Sauerbrey equation at solid–air interface after the cyanobacteria attachment. (C) Optical microscopy and AFM topography images of the QCM-D sensor surfaces showing the structural details and attached cyanobacteria filaments on TEMPO CNF.

contact of cells and matrix from at least one direction, this allows the accurate control of nutrient distribution and gas exchange between the cells and environment is readily facilitated, especially for monolayer cell structures. Direct attachment is considered to be particularly beneficial for cyanobacteria and green algae that often experience oxidative stress due to excessive and unwanted photosynthetic O_2 production.[19,48]

In order to further improve the immobilization matrix towards direct cell attachment, the CNF surface properties needed to be adapted, whilst retaining film forming capacity and optical transparency. This could be achieved using a simple surface modification route involving the adsorption of oppositely charged polyelectrolyte on TEMPO CNF surface. Here, polyethylene imine (PEI) was utilised to cationize the TEMPO CNF surface in order to improve the attachment of cyanobacteria *via* electrostatic attraction. The surface interactions between PEI-cationized TEMPO CNF thin films and Δ*hupL* filaments were investigated with the QCM-D Open module, in exactly the same approach used for anionic TEMPO CNF. As hypothesized, the change in frequency after cyanobacteria introduction was significantly larger than with anionic TEMPO CNF (Fig. 6). Within 2 h, a frequency change of approximately −27 Hz was recorded, along with a rather large positive dissipation change of 6×10^{-6}. A moderately low but significant frequency change coupled with such a high dissipation change indicate that a rather soft and uneven layer is formed on the cationized TEMPO CNF surface. Furthermore, the rinsing with pure buffer solution did not generate any further signal changes, indicating that the layer is at least moderately attached on the surface *i.e.* it remains intact despite the mechanical stress caused by the rinsing step.

The same sensor was again analysed under dry conditions, before and after the cyanobacteria attachment measurement. Interestingly, the frequency changes assessed at the solid–air interface resulted in a considerably larger areal mass change, being as high as 27 000 ng cm^{-2}. The changes in frequency and areal mass at the solid–air interface in fact exceeded the sensitivity limits of the QCM-D instrument. This substantial difference between the results observed at the solid–liquid and solid–air interfaces suggests that during the removal of liquid, other phenomena besides pure surface forces positively contribute to the attachment of cyanobacteria filaments to the cationized TEMPO CNF surface. It seems that once the filaments contact the cationic cellulose nanofibrils, they strongly attach to the fibril surface. The same remarkable difference is visually represented in the optical microscopy images (Fig. 6C). Only a few attached cyanobacterial filaments are visible on the

anionic TEMPO CNF surface, whereas significantly larger amount of filaments can be seen on the cationized TEMPO CNF surface. Moreover, AFM topography images taken from the regions between the filaments reveal the fine structure of the surfaces. Small granular particles which are likely initially adsorbed *via* attractive surface forces are presumably extracellular polysaccharides and other macromolecules secreted by the cyanobacteria. The majority of the large filaments are attached *via* oppositely charged sites but only once direct contact is achieved, for example during the removal of buffer. This attachment, taking place on several levels, can be considered as beneficial to immobilization approaches where drying is involved.

Conclusions

Immobilization matrices for the photosynthetic microbial production of H_2 were fabricated using TEMPO-oxidised cellulose nanofibrils with different strategies employed to enhance the matrix water stability. We showed that these versatile templates display high compatibility with oxygenic phototrophic organisms, and that they are suitable for thin-layer cell entrapments both in hydrogel and dry solid film states. They possess several advantageous features, which make them more attractive than other natural matrix materials. Beyond their demonstrated suitability to maintaining cellular photosynthetic activity and H_2 production capacity, constructed TEMPO CNF matrices are also mechanically stable under wet conditions, transparent and have nanoscale porosity. As a material, CNF is abundant, renewable and biodegradable. To further tailor the system towards direct cell attachment, only a simple interfacial tailoring with cationic polyelectrolyte is needed. These findings will facilitate the development of cost-effective approaches to large-scale bio-industrial applications.

Conflicts of interest

There are no conflicts to declare.

Acknowledgements

The study is financially supported by Novo Nordisk Fonden (project #NNF16OC0021626), the NordForsk NCoE program "NordAqua"(project # 82845) and the Academy of Finland (FCoE program 307335). We are thankful to Ms Katja Pettersson for help in AFM imaging.

Notes and references

1 R. H. Wijffels, O. Kruse and K. J. Hellingwerf, *Curr. Opin. Biotechnol.*, 2013, **24**, 405–413.
2 L. Zhu, *Renewable Sustainable Energy Rev.*, 2015, **41**, 1376–1384.
3 P. Patrikainen, V. Carbonell, K. Thiel, E. M. Aro and P. Kallio, *Metab. Eng. Commun.*, 2017, **5**, 9–18.
4 R. Slade and A. Bauen, *Biomass Bioenergy*, 2013, **53**, 29–38.
5 S. Singh, S. Jain, V. Ps, A. K. Tiwari, M. R. Nouni, J. K. Pandey and S. Goel, *Renewable Sustainable Energy Rev.*, 2015, **51**, 623–633.
6 H. Sakurai, H. Masukawa, M. Kitashima and K. Inoue, *Life*, 2015, **5**, 997–1018.
7 I. Akkerman, M. Janssen, J. Rocha and R. H. Wijffels, *Int. J. Hydrogen Energy*, 2002, **27**, 1195–1208.
8 M. L. Ghirardi, A. Dubini, J. Yu and P.-C. Maness, *Chem. Soc. Rev.*, 2009, **38**, 52–61.
9 M. C. Flickinger, J. L. Schottel, D. R. Bond, A. Aksan and L. E. Scriven, *Biotechnol. Prog.*, 2007, **23**, 2–17.
10 S. N. Kosourov, M. He, Y. Allahverdiyeva and M. Seibert, in *Microalgal Hydrogen Production: Achievements and Prospectives*, ed. M. Seibert and G. Torzillo, The Royal Society of Chemistry, 2018.
11 J. L. Gosse, B. J. Engel, J. C.-H. Hui, C. S. Harwood and M. C. Flickinger, *Biotechnol. Prog.*, 2010, **26**, 907–918.
12 T. V. Laurinavichene, S. N. Kosourov, M. L. Ghirardi, M. Seibert and A. A. Tsygankov, *J. Biotechnol.*, 2008, **134**, 275–277.
13 J. L. Gosse, B. J. Engel, F. E. Rey, C. S. Harwood, L. E. Scriven and M. C. Flickinger, *Biotechnol. Prog.*, 2007, **23**, 124–130.
14 S. N. Kosourov and M. Seibert, *Biotechnol. Bioeng.*, 2009, **102**, 50–58.
15 W. Song, N. Rashid, W. Choi and K. Lee, *Bioresour. Technol.*, 2011, **102**, 8676–8681.
16 H. Leino, S. N. Kosourov, L. Saari, K. Sivonen, A. A. Tsygankov, E. M. Aro and Y. Allahverdiyeva, *Int. J. Hydrogen Energy*, 2012, **37**, 151–161.
17 E. Touloupakis, G. Rontogiannis, A. M. Silva Benavides, B. Cicchi, D. F. Ghanotakis and G. Torzillo, *Int. J. Hydrogen Energy*, 2016, **41**, 15181–15186.
18 O. I. Bernal, C. B. Mooney and M. C. Flickinger, *Biotechnol. Bioeng.*, 2014, **111**, 1993–2008.
19 S. Kosourov, G. Murukesan, M. Seibert and Y. Allahverdiyeva, *Algal Res.*, 2017, **28**, 253–263.
20 D. Klemm, F. Kramer, S. Moritz, T. Lindström, M. Ankerfors, D. Gray and A. Dorris, *Angew. Chem., Int. Ed.*, 2011, **50**, 5438–5466.
21 T. Saito, Y. Nishiyama, J. L. Putaux, M. Vignon and A. Isogai, *Biomacromolecules*, 2006, **7**, 1687–1691.
22 H. Fukuzumi, T. Saito, T. Iwata, Y. Kumamoto and A. Isogai, *Biomacromolecules*, 2009, **10**, 162–165.
23 T. Mäkelä, M. Kainlauri, P. Willberg-Keyriläinen, T. Tammelin and U. Forsström, *Microelectron. Eng.*, 2016, **163**, 1–6.
24 S. Arola, T. Tammelin, H. Setälä, A. Tullila and M. B. Linder, *Biomacromolecules*, 2012, **13**, 594–603.
25 M. Jorfi and E. J. Foster, *J. Appl. Polym. Sci.*, 2015, **132**, 1–19.
26 A. Mautner, K.-Y. Lee, P. Lahtinen, M. Hakalahti, T. Tammelin, K. Li and A. Bismarck, *Chem. Commun.*, 2014, **50**, 5778–5781.
27 H. Dong, J. F. Snyder, K. S. Williams and J. W. Andzelm, *Biomacromolecules*, 2013, **14**, 3338–3345.
28 M. Hakalahti, A. Salminen, J. Seppälä, T. Tammelin and T. Hänninen, *Carbohydr. Polym.*, 2015, **126**, 78–82.

29 M. Vuoriluoto, H. Orelma, M. Lundahl, M. Borghei and O. J. Rojas, *Biomacromolecules*, 2017, **18**, 1803–1813.
30 H. Masukawa, M. Mochimaru and H. Sakurai, *Appl. Microbiol. Biotechnol.*, 2002, **58**, 618–624.
31 J. Kotai, *Instructions for preparation of modified, nutrient solution Z8 for algae. Publication B-11/69*, Norwegian Institute for Water Research, Oslo, 1972.
32 E. H. Harris, *The Chlamydomonas sourcebook: a comprehensive guide to biology and laboratory use*, Academic Press, San Diego, 1989.
33 A. Melis, L. Zhang, M. Forestier, M. L. Ghirardi and M. Seibert, *Plant Physiol.*, 2000, **122**, 127–136.
34 M. Hakalahti, M. Faustini, C. Boissière, E. Kontturi and T. Tammelin, *Biomacromolecules*, 2017, **18**, 2951–2958.
35 M. Rodahl, F. Höök, A. Krozer, P. Brzezinski and B. Kasemo, *Rev. Sci. Instrum.*, 1995, **66**, 3924–3930.
36 F. Höök, M. Rodahl, P. Brzezinski and B. Kasemo, *Langmuir*, 1998, **14**, 729–734.
37 P. Eronen, K. Junka, J. Laine and M. Österberg, *BioResources*, 2011, **6**, 4200–4217.
38 M. S. Peresin, K. Kammiovirta, H. Setälä and T. Tammelin, *J. Polym. Environ.*, 2012, **20**, 895–904.
39 H. K. Lichtenthaler, *Methods Enzymol.*, 1987, **148**, 350–382.
40 S. N. Kosourov, K. A. Batyrova, E. P. Petushkova, A. A. Tsygankov, M. L. Ghirardi and M. Seibert, *Int. J. Hydrogen Energy*, 2012, **37**, 8850–8858.
41 A. Scoma and A. Hemschemeier, *Algal Res.*, 2017, **26**, 341–347.
42 M. Hirai, R. Yamakawa, J. Nishio, T. Yamaji, Y. Kashino, H. Koike and K. Satoh, *Plant Cell Physiol.*, 2004, **45**, 872–878.
43 A. Isogai, T. Saito and H. Fukuzumi, *Nanoscale*, 2011, **3**, 71–85.
44 S. V. Lalonde, D. S. Smith, G. W. Owttrim and K. O. Konhauser, *Geochim. Cosmochim. Acta*, 2008, **72**, 1269–1280.
45 S. F. Karel, S. B. Libicki and C. R. Robertson, *Chem. Eng. Sci.*, 1985, **40**, 1321–1354.
46 S. F. Dagher, A. L. Ragout, F. Siñeriz and J. M. Bruno-Bárcena, *Adv. Appl. Microbiol.*, 2010, 113–148.
47 T. A. Smirnova, L. V. Didenko, R. R. Azizbekyan and Y. M. Romanova, *Microbiology*, 2010, **79**, 413–423.
48 K. Hakkila, T. Antal, A. U. Rehman, J. Kurkela, H. Wada, I. Vass, E. Tyystjärvi and T. Tyystjärvi, *Biochim. Biophys. Acta, Bioenerg.*, 2014, **1837**, 217–225.